Geol. Mag. **141** (*4*), *2004, pp. 417–428. © 2004 Cambridge University Press*
DOI: 10.1017/S0016756804009392 *Printed in the United Kingdom*

Probing the Vesuvius magma chamber–host rock interface through xenoliths

P. FULIGNATI, P. MARIANELLI, R. SANTACROCE & A. SBRANA*

Dipartimento di Scienze della Terra, Via S. Maria 53, 56126 Pisa, Italy

(*Received* 11 August 2003; *accepted* 27 March 2004)

Abstract – The thermal and compositional conditions of magma chambers constrain the type and complexity of their metasomatic aureoles. Fragments of these aureoles, disrupted during explosive eruptions of Vesuvius, provide quenched snapshots of interactions between potassic magmas and carbonate country rocks. Near the highly crystallized peripheral portions of the chambers, represented by magmatic xenoliths (fergusites, syenites and pyroxenites), skarn aureoles form. Open conduit reservoirs and the lower portions of plinian and subplinian eruption magma chambers develop aureoles controlled by diffusive metasomatism by high-*T*-modified silicate melts, generating magmatic skarn. In contrast, infiltrative metasomatism by magmatic fluids exsolved from crystallizing margins is responsible for endoskarn (magmatic protolith) and exoskarn (carbonate protolith) formation in the upper portions of plinian and subplinian eruption magma chambers.

Keywords: Vesuvius, magma chamber, skarn, melt inclusions, fluid inclusions.

1. Introduction

The emplacement of hot silicate magmas into the crust results in the formation of magma chambers followed by magma cooling, crystallization, degassing and reaction with host rocks. In the case of carbonate host rocks (limestone and dolostone), the composition of magmas and host rocks can undergo significant changes due to complex interactions. This is reflected in the formation of metasomatic aureoles, at the magma chamber–host carbonate interface, that are generally termed skarns (Einaudi, Meinert & Newberry, 1981; Meinert, 1992, 1993). As skarns may host certain ores (e.g. Au, Cu, Fe, Mo, Sn, W, Zn, Pb), their chemical diversity has long been the subject of economic geology studies, and their genetic mechanisms have been widely investigated in skarn aureoles associated with exposed intrusive bodies (Einaudi, Meinert & Newberry, 1981; Burt, 1982; Meinert, 1992, 1993; Lentz, 1998). Fundamental research into the origin and composition of skarns has recently benefited from a new approach based on mineralogical, and melt and fluid inclusion studies of rocks that formed the magma chamber walls and which have been delivered to the surface as compact nodules (xenoliths) in explosive eruptions (Cortini, Lima & De Vivo, 1985; Belkin *et al*. 1985; Belkin & De Vivo, 1993; Matthews *et al*. 1996; Fulignati, Marianelli & Sbrana, 2000; Fulignati *et al*. 2000, 2001; Gilg *et al*. 2001; Lima *et al*. 2003). Because of their quenched nature, xenoliths can be seen as frozen snapshots of the different degrees of interaction that occurred at different moments in the magma chamber, mirroring skarn halo evolution, without any retrograde effects obliterating the previously occurring processes.

The objective here is to constrain the relationships existing between the development of skarn aureoles and of magma chambers characterized by different temperatures and compositions, that were active during the history of Vesuvius, through the investigation of erupted xenoliths. Vesuvius is particularly suitable for this because its shallow magmatic system (< 6 km) is hosted within carbonate rocks, and the physical-chemical conditions of magma chambers can be relatively well defined (Barberi *et al*. 1981; Santacroce *et al*. 1993; Belkin & De Vivo, 1993; Cioni *et al*. 1995; Cioni, Marianelli & Santacroce, 1998; Marianelli, Metrich & Sbrana, 1999; Cioni, 2000; Lima *et al*. 2003). For this purpose, three eruptions (1944, AD 472 'Pollena', and AD 79 'Pompei') that are representative of the variability of Vesuvian explosive activity (effusive to violent strombolian, subplinian and plinian) were selected. Vesuvian magma chambers form and grow through the periodic arrival of K-tephritic magma batches and expand mainly laterally, decreasing their aspect ratio (height/width). The increasing volume of the resident magma is accompanied by changes in compositional layering as well as in the thermal state of the chambers (Cioni, Marianelli & Santacroce, 1998). The three eruptions are assumed, on the basis of previous works (Cioni, Marianelli & Santacroce, 1998; Marianelli, Metrich & Sbrana, 1999), to result from the emptying of shallow magma chambers having reached different sizes, stages of evolution and composition (Fig. 1) of magmas: open conduit, small-sized 'early' (1944), 'young' (AD 472) and 'mature' (AD 79). The 1944 eruption was fed by an open conduit shallow

* Author for correspondence: sbrana@dst.unipi.it

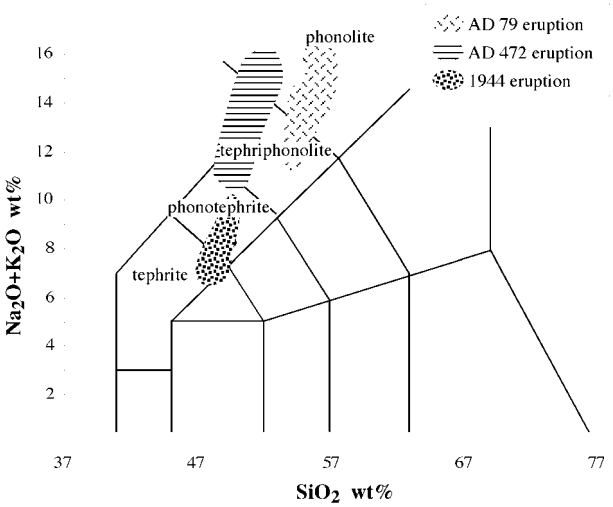

Figure 1. Total Alkali v. Silica diagram (Le Bas *et al*. 1986) of juvenile products from selected Vesuvius eruptions. Data from Cioni, Marianelli & Santacroce (1998) and Marianelli, Metrich & Sbrana (1999).

reservoir of small volume (< 0.1–0.2 km^3) filled by homogeneous mafic magma ($T > 1050$ °C), crystal-enriched downward, and with high aspect ratio (Marianelli, Metrich & Sbrana, 1999). The AD 472 magma chamber is characterized by both medium volume and a moderate aspect ratio, and continuous compositional gradation from top felsic (850–900 °C) to bottom mafic (1050–1100 °C) melts ('young' magma chamber), as hypothesized by Cioni, Marianelli & Santacroce (1998). The AD 79 magma chamber is viewed as a large (> 1 km^3), subequant (low aspect ratio), twofold reservoir with a stepwise compositional gradient separating a low, convective, mildly evolved (*c*. 1050 °C) magma from an upper, stratified, salic layer (800–900 °C) ('mature' magma chamber: Cioni, Marianelli & Santacroce, 1998).

2. Methods

Analyses of minerals, unheated melt inclusions and interstitial glasses were carried out by Energy Dispersive Scanning Electron Microscopy (SEM-EDS) at Dipartimento di Scienze della Terra, University of Pisa (Philips XL30 equipped with EDAX DX4), at 20 kV accelerating energy and about 0.1 nA beam current. A raster area of about 100 μm^2 was employed for glass analysis to reduce light element loss. Analyses are normalized to 100% due to the EDAX software used. Before each session the quality of analyses was checked using certified minerals and glasses as reference standards. Accuracy and precision on each oxide and standard used are reported in Marianelli & Sbrana (1998). For the high-temperature experiments on fluid and melt inclusions a Linkam TS 1500 heating stage and an optical heating stage, designed in the Vernadsky Institute of Geochemistry, Moscow (described by Sobolev *et al*. 1980), were used. The accuracy of measurement was around ± 10 °C for both heating stages, controlled by the melting point of pure silver and gold and $K_2Cr_2O_7$.

3. Petrography and mineralogy

Xenoliths from the disruption of magma chamber walls are relatively common in the deposits of Vesuvius eruptions. This paper presents new data on well-preserved glasses, and melt and fluid inclusions in crystals in selected samples. These xenoliths include highly crystallized rocks representative of the outer margins of the magma chambers: glass-bearing fergusites (1944 eruption), foid-bearing K-syenites (AD 472 and AD 79 eruptions), and cumulus clinopyroxenites (all three eruptions), as well as skarn (all three eruptions).

A nearly complete chemical and mineralogical gradation of glass-bearing fergusites and foid-bearing syenites to salite-bearing clinopyroxenites is observed. The sharp contact between skarn and foid-bearing syenites (AD 79) or glass-bearing fergusites (1944) or clinopyroxenites (AD 79, AD 472, 1944) is sometimes seen in collected ejecta. Furthermore, widespread skarn veins are commonly found in several AD 79 marble xenoliths.

3.a. Magmatic xenoliths

Cumulus clinopyroxenite xenoliths are found in all three eruption deposits. They consist of subeuhedral to euhedral clinopyroxene, very subordinate olivine and partially crystallized interstitial glass. In 1944 clinopyroxene-rich nodules, the clinopyroxenes (Table 1) are either unzoned ($Wo_{47}Fs_5$) or zoned with small diopsidic cores ($Wo_{47}Fs_5$) surrounded by very thick salitic rims ($Wo_{50}Fs_{11}$). In xenoliths erupted in AD 79 and AD 472, only diopsidic clinopyroxenes (Table 1) were found ($Wo_{46-49}Fs_{5-7}$).

Another type of magmatic xenolith is represented by glass-bearing fergusites that are found in 1944 deposits. They are made of a cumulus crystal framework (leucite, clinopyroxene $Wo_{49-50}Fs_{13-17}$ (Table 1)), plagioclase, olivine, Fe–Ti oxides with minor apatite and interstitial glassy matrix. Melt inclusions and glassy matrix compositions are variable and range from K-phonotephrite (similar to glassy matrix of juvenile scoriae) to more evolved K-tephriphonolite.

The third type of magmatic xenolith is represented by foid-bearing syenites present only in AD 472 and AD 79 deposits. These are nearly holocrystalline (AD 472) to hypohyaline with K-phonolitic interstitial glass (AD 79), nonequigranular rocks consisting of a network of euhedral crystals of K-feldspar and leucite (abundant in AD 472); other constituents are nepheline, K-pargasitic amphibole, garnet, salitic clinopyroxene (only in AD 472 samples, Table 1) and biotite. The AD 79 foid-bearing syenites are further distinguished from AD 472 ones by the abundance of accessories. In

https://doi.org/10.1017/S0016756804009392 Published online by Cambridge University Press

Table 1. Representative analyses of clinopyroxenes from the different types of Vesuvius xenoliths

Rock type	SK	SK	SK	SK	SK	SK	SK	C	C	C	C	F	S	S
Eruption	AD 79 unzoned	AD 79 unzoned	AD 472 core	AD 472 rim	AD 472 unzoned	1944 core	1944 rim	AD 79 unzoned	AD 472 unzoned	1944 core	1944 rim	1944 unzoned	AD 472 core	AD 472 rim
SiO_2	43.56	47.16	46.38	47.71	41.19	44.26	41.78	53.31	52.75	53.43	48.12	48.62	45.48	41.17
TiO_2	1.37	0.89	1.16	1.41	0.97	1.87	2.52	0.22	0.34	0.22	1.07	1.16	1.56	2.81
Al_2O_3	9.98	7.44	7.97	7.86	17.17	10.16	13.44	1.66	1.85	1.28	6.93	5.64	7.55	10.45
FeO_{tot}	11.84	2.24	8.53	2.91	5.06	7.28	5.78	3.44	3.62	3.23	6.35	9.00	10.75	16.03
MnO	0.21	0.12	b.d.l.	b.d.l.	b.d.l.	0.20	b.d.l.	b.d.l.	0.05	0.12	0.16	0.15	0.38	0.66
MgO	8.47	15.19	11.64	14.36	10.17	11.98	11.23	16.83	16.69	17.72	13.22	12.15	9.72	5.29
CaO	23.56	26.73	23.96	25.63	25.34	23.87	25.11	24.32	24.41	23.77	23.92	22.91	24.07	22.86
Na_2O	1.01	0.23	0.36	0.12	0.10	0.38	0.14	0.22	0.29	0.23	0.23	0.37	0.49	0.73
Total	100.00	100.00	100.00	100.00	100.00	100.00	100.00	100.00	100.00	100.00	100.00	100.00	100.00	100.00
Wo	52.80	53.90	51.20	53.50	58.30	51.60	55.40	48.23	48.34	46.63	50.58	48.88	0.65	1.09
En	26.40	42.60	34.60	41.70	32.60	36.10	34.60	46.45	46.05	48.42	38.92	36.11	18.48	26.42
Fs	20.70	3.50	14.20	4.70	9.10	12.30	10.00	5.32	5.60	4.95	10.50	15.05	80.87	72.49

Rock type: SK – skarn; C – cumulus clinopyroxenites; F – glass-bearing fergusites; S – foid-bearing syenites. Analyses are normalized to 100 due to the EDAX software used. b.d.l. – below detection limit. Reported analyses are selected from a set of more than 250 analyses (the complete data set will be available upon request).

particular, they are characterized by the occurrence of fluorite, sodalite and REE and HFSE-bearing minerals such as monazite, thorite and dysanalite.

3.b. Skarn xenoliths

Skarn xenoliths found in all three eruption deposits show a hetero- to homogranular texture. Some samples show the occurrence of interstitial glass. On the whole, the mineralogy of these ejecta is typical of skarn rocks, being characterized by the presence of fassaitic clinopyroxene ($Wo_{55-52}Fs_{13-5}$, Table 1) associated with variable amounts of phlogopite, melilite, olivine and spinel, as well as sporadic plagioclase, garnet, nepheline and periclase. Skarn xenoliths, with abundant phlogopite, are common in all three eruptions, whereas melilite characterizes part of the skarn xenoliths found in 1944 and AD 472 eruption deposits. Another mineralogical peculiarity that characterizes some skarn xenoliths of 1944 and AD 472 eruptions is represented by the occurrence of clinopyroxenes that exhibit cores having compositions coincident with juvenile salitic pyroxenes ($Wo_{50-51}Fs_{12-14}$, Table 1), and fassaitic rims. These cores can be considered as relicts of magmatic clinopyroxenes. Skarn xenoliths of the AD 79 eruption are characterized by a calc-silicate mineralogical assemblage often associated with calcite crystals.

4. Melt and fluid inclusions

4.a. Cumulus clinopyroxenite

Melt inclusions, present in cumulus clinopyroxenites of all three eruption deposits, generally appear opaque due to the presence of crystal nuclei and thermometric experiments were not carried out on these.

4.b. Glass-bearing fergusite

Crystals of plagioclase, leucite and apatite contain primary two-phase melt inclusions (brown glass + shrinkage bubble). Melt inclusion composition ranges from K-phonotephrite to K-tephriphonolite and is similar to the composition of the glassy matrix. The temperature of these melts has been estimated to be about 1050 °C (Fulignati, Marianelli & Sbrana, 2000).

4.c. Foid-bearing syenites

4.c.1. Melt inclusions

Melt inclusions, found in AD 472 foid-bearing syenites, consist of silicate glass ± one or more fluid-bearing globules containing a vapour bubble and daughter minerals. The glass/globule ratio is highly variable and in many inclusions fluid-bearing globules are prevalent (Fulignati *et al*. 2001). Similar melt inclusions (silicate glass + daughter minerals + vapour bubble ± liquid phase) were also found in AD 79 foid-bearing syenites.

The strong variability of the glass/hypersaline fluid phase ratio, found in these AD 472 and AD 79 multiphase inclusions, is interpreted as strong evidence that silicate melt and saline fluids coexisted and were trapped heterogeneously (Roedder, 1992; Lowenstern, 1995; Kamenetsky *et al*. 2003). Thermometric experiments carried out on AD 79 multiphase melt inclusions show that glass begins to melt at about 600 °C, while the temperature of disappearance of cubic daughter mineral (halite) is always above 500 °C, revealing high salinity. Complete homogenization is rarely reached at high temperatures (∼970 °C, Table 2) that are obviously unrealistic.

4.c.2. Hypersaline fluid inclusions

Hypersaline fluid inclusions were found in foid-bearing syenites both from AD 472 and AD 79 eruptions. These inclusions consist of a vapour bubble, a liquid phase and several daughter minerals. In AD 79 samples the last cubic daughter mineral (halite) dissolves at temperatures from 515 °C to 570 °C, corresponding to salinity of 62–66 wt % $NaCl_{equiv}$, and the temperature of homogenization of the vapour bubble in the liquid phase occurs in the interval 760–880 °C (Table 2). Hypersaline fluid

https://doi.org/10.1017/S0016756804009392 Published online by Cambridge University Press

Table 2. Summary of melt and fluid inclusion data

Samples	Type of inclusions	Salinity (NaCl wt % $_{equiv}$)[a]	Temperature of homogenization
AD 79 foid-bearing syenites	Multiphase melt inclusions	52–80 [N = 30]	970–980 °C[d] [N = 3]
	Hypersaline fluid inclusions	62–66 [N = 30]	T = 760–880 °C [N = 30]
AD 79 cumulus clinopyroxenite	Melt inclusions	–	–
AD 79 skarn	Hypersaline fluid inclusions	52–58 [N = 22]	T = 800–850 °C [N = 22]
AD 472 foid-bearing syenites	Multiphase melt inclusions	–	–
	Hypersaline fluid inclusions	61–72[b] [N = 70]	T = 700–850 °C[b] [N = 95]
AD 472 cumulus clinopyroxenite	Melt inclusions	–	–
AD 472 skarn	Multiphase (carbonate-bearing) melt inclusions	Very high[c]	T = 860–885 °C[e] [N = 5]
1944 glass-bearing fergusites	Melt inclusions	–	–
1944 cumulus clinopyroxenite	Melt inclusions	–	–
1944 skarn	Melt inclusions	–	T = 800–920 °C / 1010–1033 °C [N = 24]
	Multiphase (silicate-bearing) melt inclusions	73–77 [N = 9]	T = 1228 °C[d] [N = 2]

[a] The multiphase inclusions found either in foid-bearing syenites and in skarn xenoliths reflect very complex systems in which, in addition to chlorides, other components are also present (carbonates, sulphates, fluorides, Fulignati *et al.* 2001, 2004). As a consequence, the salinity calculated according to Sterner, Hall & Bodnar (1988) and expressed in terms of wt % $NaCl_{equiv}$ is only approximate. This is clearly indicated by the temperature of disappearance (in excess of 800 °C) of halite in hydrosaline carbonate-bearing inclusions of AD 472 skarn, which is higher than the value (800 °C) for 100 wt % pure NaCl (Sterner, Hall & Bodnar, 1988).
[b] Data from Fulignati *et al.* (2001) and this work.
[c] The temperature of disappearance of the last cubic (halite?) daughter mineral is between 800–830 °C (N = 120: data from Fulignati *et al.* 2001 and this work); as a consequence the salinity expressed in wt % $NaCl_{equiv}$ cannot be calculated.
[d] These temperatures of homogenization are unrealistic because these inclusions record the entrapment of immiscible silicate melt and hypersaline fluids.
[e] These values are probably overestimated due to deformation of the cavity of the inclusions during heating experiments.

inclusions in AD 472 foid-bearing syenites have a temperature of disappearance of the cubic daughter mineral of 510–590 °C, corresponding to a salinity ranging from 61 to 72 wt % $NaCl_{equiv}$. The temperature of homogenization of the vapour bubble in the liquid phase always occurs after the disappearance of salts at temperatures from 700 °C to 850 °C (Table 2).

4.d. Skarn

4.d.1. Melt inclusions and interstitial glasses

Among selected skarn xenoliths of all three eruptions, some are characterized by the occurrence of interstitial glasses and crystals with silicate glassy inclusions (Fig. 2a). Silicate melt inclusions in skarn minerals are rare and have been recognized only recently (Zhao & Zhao, 1996; Zhao & Newberry, 1996; Zhao, Zhao & Li, 2000; Fulignati *et al*. 2000; Lima *et al*. 2003). In the 1944 studied samples, melt inclusions (glass + shrinkage bubble ± carbonate solids) are hosted within clinopyroxene, plagioclase and rarely melilite. They show high temperatures of homogenization ranging from 800 °C to 920 °C (phlogopite-bearing paragenesis) and 1010 °C to 1030 °C (melilite-bearing paragenesis, Table 2).

Silicate melt inclusions and interstitial glasses from all three eruptions have exotic compositions (Table 3) showing strong Ca (and Mg) enrichment when compared with Vesuvian K-tephritic to K-phonolitic melts (Fig. 3). The potential influence of post-entrapment of the host phase on the chemistry of unheated silicate melt inclusions has been addressed following the procedure reported in Webster *et al*. (2001). The outcome of this approach indicates that compositional trends shown by melt inclusions are independent of the post-trapping host phase crystallization.

Multiphase melt inclusions (silicate glass + liquid phase + daughter minerals) were rarely found in some 1944 phlogopite-bearing skarn xenoliths. Salts disappear at 595–624 °C, indicating salinity from 73 to 77 wt% $NaCl_{equiv}$ (Table 2). At 880 °C the glass is completely molten. Complete homogenization is reached only in a few inclusions at very high temperatures (> 1200 °C, Table 2). These unrealistic high temperatures and the variability of the glass/salts ratio make it evident that, in this case, inclusions do not give any indication of the trapping temperature. Conversely, they record evidence for entrapment of immiscible silicate melt and hypersaline liquids.

https://doi.org/10.1017/S0016756804009392 Published online by Cambridge University Press

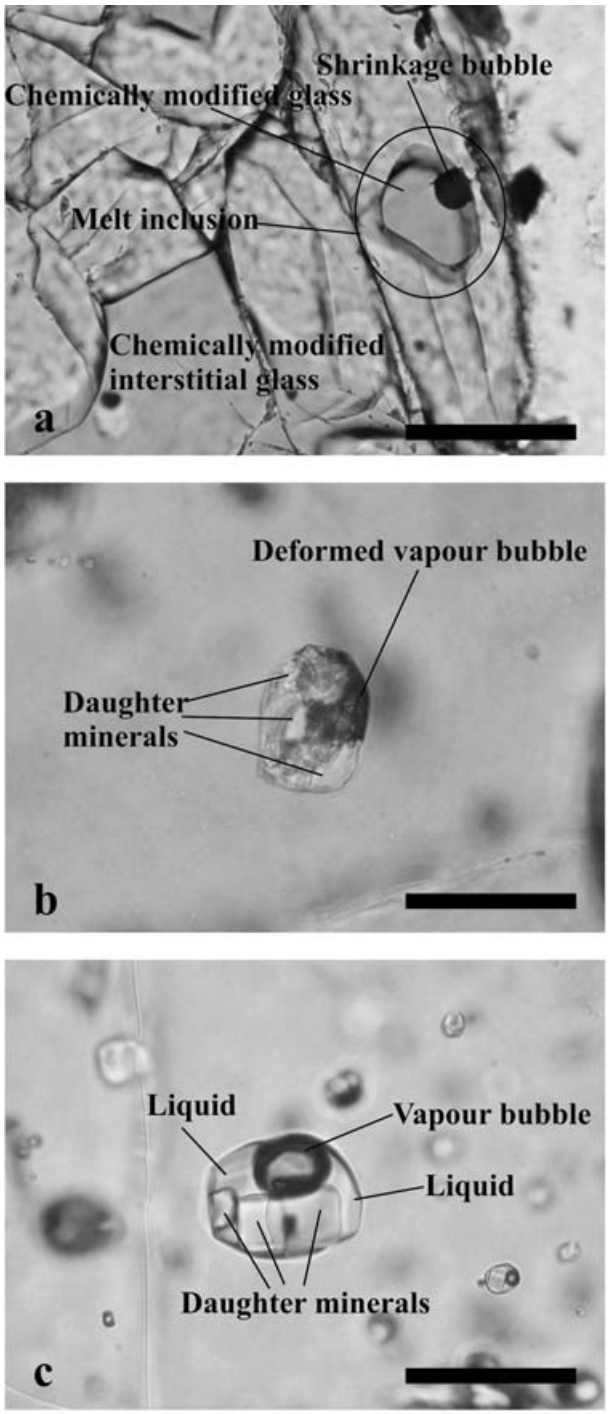

Figure 2. Representative fluid inclusions in skarn minerals. (a) Silicate two-phase (glass + shrinkage bubble) melt inclusion hosted within fassaitic clinopyroxene and interstitial glasses from magmatic skarn of the 1944 eruption. (b) Multiphase (carbonate-bearing) melt inclusions containing daughter minerals and a deformed vapour bubble hosted within nepheline from endoskarn of the AD 472 eruption. Daughter mineral paragenesis is dominated by carbonates with minor chlorides. (c) Hypersaline fluid inclusion containing daughter minerals, vapour bubble, and liquid hosted within fassaitic clinopyroxene from exoskarn of the AD 79 eruption. Daughter mineral paragenesis dominated by chlorides. All scale bars are 40 μm.

4.d.2. Multiphase (carbonate-bearing) melt inclusions

Some skarn xenoliths of the AD 472 eruption are characterized by the presence of multiphase (carbonate-bearing) melt inclusions (deformed vapour bubble + carbonate and chloride-bearing daughter minerals) (Fulignati *et al*. 2001) hosted in nepheline crystals (Fig. 2b). These inclusions proved problematic in conventional microthermometric studies and the majority decrepitated before homogenization on heating. The homogenization temperature was obtained only in very few inclusions (in the range 860°–885 °C, Table 2), and these values are probably overestimated due to deformation of the cavity of the inclusions during heating experiments. The last cubic daughter mineral (halite) always disappears at temperatures greater than 800 °C (Fulignati *et al*. 2001).

4.d.3. Hypersaline fluid inclusions

In skarn xenoliths from the AD 79 eruption only hypersaline fluid inclusions (vapour bubble + chloride bearing daughter minerals + liquid) were found. They are hosted in fassaitic clinopyroxene. Cubic daughter minerals (halite) disappear at a temperature ranging from 440 °C to 490 °C, corresponding to salinity of 55–60 wt% $NaCl_{equiv}$ (Fig. 2c, Table 2). The temperature of homogenization of the vapour bubble in the liquid phase is in the range of 800–850 °C.

5. Discussion

The feeding system of Vesuvius is characterized by the presence of shallow (< 6 km) magma chambers hosted within carbonate units (Barberi & Leoni, 1980; Belkin & De Vivo, 1993; Cioni, Marianelli & Santacroce, 1998; Marianelli, Metrich & Sbrana, 1999; Fulignati *et al*. 2000). The challenge is to use magmatic and skarn xenoliths to obtain information about the magma chamber–host rock interface in three Vesuvius eruptions that are representative of the variability of Vesuvian explosive activity.

5.a. Magma chamber solidification front

The occurrence of magmatic xenoliths such as clinopyroxenites, glass-bearing fergusites and foid-bearing syenites strongly suggests the presence in these magma chambers of a solidification front. This should be considered as a dynamic environment, propagating inward and thickening with time (Marsh, 1995). In the case of Vesuvius, the refilling of the chamber with tephritic magmas (Marianelli *et al*. 1995) conditions the development of the solidification front, preventing or reducing the thickening of crystallized margins that can be envisaged as the effective wall rock of the magma chamber (‘rigid crust’: Marsh, 1995).

https://doi.org/10.1017/S0016756804009392 Published online by Cambridge University Press

Table 3. Selected analyses of melt inclusions and interstitial glasses found in magmatic skarn xenoliths

	SiO_2	TiO_2	Al_2O_3	FeO_{tot}	MnO	MgO	CaO	Na_2O	K_2O	P_2O_5	Cl
1944 eruption											
Melt inclusion	42.62	1.99	19.20	8.24	0.28	3.03	9.57	3.92	8.93	1.27	0.95
Melt inclusion	40.85	0.51	18.77	9.26	0.50	3.07	16.27	3.82	5.52	0.57	0.86
Melt inclusion	41.83	1.51	17.76	11.24	0.23	3.76	12.22	3.04	5.69	1.42	1.30
Melt inclusion	43.88	1.13	16.56	11.08	0.35	3.78	11.01	3.39	6.81	0.96	1.05
Melt inclusion	48.14	1.02	20.37	9.64	0.24	1.78	5.34	5.27	6.84	0.52	0.84
Interstitial glass	47.35	1.21	18.82	9.68	0.36	2.32	7.67	5.34	5.96	0.45	0.84
Interstitial glass	47.20	0.78	22.07	4.14	0.18	2.56	9.17	5.06	7.74	0.28	0.82
Interstitial glass	46.94	0.92	22.54	4.04	0.17	2.66	8.92	5.18	7.47	0.37	0.79
Interstitial glass	46.92	0.78	22.09	4.00	0.26	2.87	9.35	5.13	7.36	0.42	0.82
Interstitial glass	47.23	0.53	22.14	4.11	0.17	3.53	8.68	5.20	7.31	0.28	0.82
Interstitial glass	47.04	0.28	22.24	4.16	0.23	2.55	9.68	5.11	7.52	0.31	0.88
Interstitial glass	47.03	0.26	22.13	4.43	0.20	3.04	9.03	5.20	7.68	0.12	0.88
AD 472 eruption											
Interstitial glass	43.60	0.39	20.09	5.80	0.18	4.08	14.31	2.83	7.05	0.99	0.68
Interstitial glass	38.12	0.39	14.38	3.91	0.12	7.98	30.29	1.08	2.88	0.71	0.14
Interstitial glass	37.02	0.67	14.52	4.00	0.21	7.16	31.69	1.16	2.97	0.49	0.11
Interstitial glass	36.86	0.81	12.98	3.95	0.19	10.92	29.61	1.05	3.17	0.37	0.09
Interstitial glass	36.44	0.49	13.31	4.20	0.16	7.59	33.34	1.15	2.39	0.69	0.24
Interstitial glass	36.73	0.81	16.60	3.86	0.40	7.86	28.20	1.24	3.57	0.58	0.15
Interstitial glass	45.41	0.46	20.39	5.94	0.24	2.79	9.94	3.37	9.45	1.23	0.78
Interstitial glass	47.31	0.69	19.61	6.37	0.32	2.86	8.87	3.25	9.22	0.83	0.67
Interstitial glass	44.52	0.17	19.93	6.38	0.36	3.77	12.03	3.27	7.89	0.89	0.79
Interstitial glass	35.78	0.61	15.40	4.68	0.30	6.63	31.22	1.39	2.57	1.09	0.33
Interstitial glass	37.54	0.80	14.91	3.71	0.21	8.45	28.94	1.27	3.63	0.37	0.17
Interstitial glass	33.30	0.59	16.22	4.33	0.60	9.16	29.08	2.00	3.61	0.84	0.27
Interstitial glass	36.79	0.40	19.14	4.20	0.47	4.71	25.75	2.35	5.13	0.70	0.36
Interstitial glass	36.88	0.22	19.21	4.05	0.37	4.41	26.35	2.51	5.02	0.53	0.45
Interstitial glass	36.32	0.08	18.61	4.10	0.35	4.32	27.13	2.68	5.40	0.48	0.53
AD 79 eruption											
Interstitial glass	47.35	0.46	24.48	5.64	0.29	1.54	7.64	3.57	7.26	0.99	0.78
Interstitial glass	46.60	0.50	24.61	4.94	0.22	1.65	10.59	3.37	6.12	0.74	0.66
Interstitial glass	48.66	0.31	25.54	4.34	0.33	1.36	6.69	3.80	7.62	0.75	0.60

Reported analyses are selected among a set of more than 100 analyses (the complete data set will be available upon request). Analyses are normalized to 100 due to the EDAX software used.

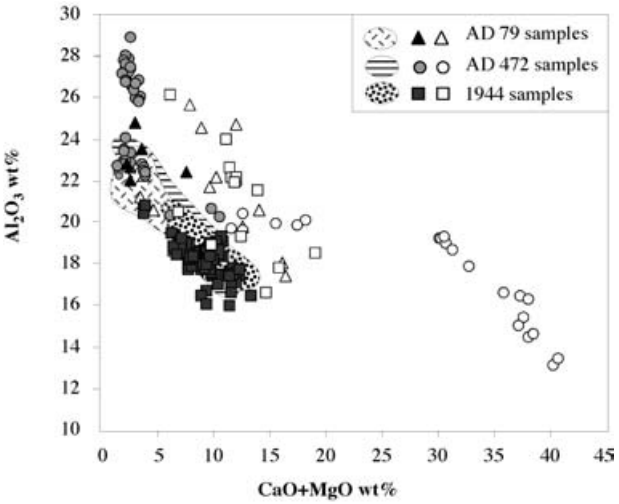

Figure 3. Al_2O_3 v. CaO + MgO diagram of interstitial glasses and silicate melt inclusions. Fields represent juvenile melt inclusions and glass matrix of the 1944, AD 472 and AD 79 eruptions (Cioni *et al*. 1995; Cioni, Marianelli & Santacroce, 1998; Marianelli, Metrich & Sbrana, 1999). Solid symbols represent silicate melt inclusions and interstitial glasses of magmatic xenoliths (clinopyroxenites, glass-bearing fergusites, and foid-bearing syenites). Open symbols represent silicate melt inclusions and interstitial glasses of skarn.

Clinopyroxenites result from the accumulation of crystals in the lower portions of magma chambers. In the case of diopside-bearing clinopyroxenites that are characteristic of AD 472 and AD 79 eruptions, crystals segregated from feeding primitive K-tephritic batches by crystallization while reaching thermal equilibrium with magma resident in the lower portion of the chamber (Marianelli *et al*. 1995). Salite-bearing clinopyroxenites can instead be envisaged as the result of accumulation of salitic clinopyroxenes formed from K-phonotephritic melt resident in the shallow reservoir of the 1944 eruption.

The solidification front in the upper parts of the magma chambers is thought to be formed by glass-bearing fergusites and foid-bearing syenites. Glass-bearing fergusites derive from differentiated portions of K-phonotephritic melts. In particular these rocks are interpreted as forming at high temperature (1050 °C) from combined sidewall accumulation of crystals of the K-phonotephritic magma, resident in the upper portion of 1944 chamber, and *in situ* evolution of the intercumulus melt (Fulignati *et al*. 2000). Foid-bearing syenites (AD 472 and AD 79) are thought to result from similar processes occurring in the upper portions of the phonolitic magma chambers at temperatures

https://doi.org/10.1017/S0016756804009392 Published online by Cambridge University Press

in the range of 750–850 °C, as deduced from fluid inclusion investigations. The foamy appearance of foid-bearing syenites can be interpreted as resulting from the crystallization of K-feldspars in the presence of exsolved fluids accumulating under the roof of the magma chambers as suggested by Lowenstern & Sinclair (1996). This is confirmed by the occurrence of hypersaline, high-*T* fluid inclusions, indicating that magmatic brines are exsolved on the walls of phonolitic magma chambers of Vesuvius. The exsolution of magmatic brines from evolved Vesuvius magmas has also been demonstrated by Webster *et al*. (2001), Webster & De Vivo (2002) and Webster, De Vivo & Tappen (2003). The direct exsolution of a hydrous chloride melt (with or without vapour) is a key difference that characterizes the upper part of the solidification fronts of 'young' (AD 472) and 'mature' (AD 79) magma chambers in respect to the 1944 solidification front, as indicated by the occurrence of hypersaline fluid inclusions only in foid-bearing syenites.

Although xenoliths cannot be uniquely associated with a specific position on the magma chamber sidewall, we envisage the margins of Vesuvian magma chambers to be vertically zoned with mafic cumulates in the deeper parts (all three eruptions), and fergusites (1944) or foid-bearing syenites (AD 472 and AD 79) in the upper parts.

5.b. Metasomatized aureole

The results of this study show that the various skarn xenoliths do not strongly differ in their mineralogy but they mainly differ in the types of melt and fluid inclusions hosted in their minerals. On the basis of melt and fluid inclusion investigation we shed light on the processes involved in the skarn genesis in the different types of magma chambers at Vesuvius.

5.b.1. Magmatic skarn

Skarns hosting melt inclusions and interstitial glass were found in all three eruption deposits. These glasses show exotic composition characterized by enrichment in Ca and Mg when compared with 'true' Vesuvian magmatic melts (Fig. 3). The anomalous compositions of glasses can be explained as resulting from the mixing of different amounts of CaO and MgO (most probably supplied by decarbonation reactions and/or melting of the carbonate) with silicate melts. These latter are assumed to be differentiated melts produced by crystallization in the solidification front of magma chambers (Fulignati *et al*. 2000). The strong crystallization occurring in this zone supplies energy for endothermic decarbonation reactions that destroys carbonate wall rock (Bowen, 1928; Joesten, 1977) increasing its porosity, and thus enhancing the infiltration of melts or fluids into the wall rocks. CaO and MgO addition to the differentiated melt has the effect of strongly lowering its viscosity down to about 7 Pa·s (the viscosity of melts is calculated from the composition of chemically modified glasses using the 'KWare Magma' software of Wohletz (2002). Viscosity varies from 7 to 30 Pa·s for compositions characterized by CaO contents ranging between 33 wt % and 16 wt % (see Fig. 4), temperature ranging between 1030 °C and 800 °C and pressure of 100 MPa). The low viscosity further enhances the mobility and infiltration capability of melts in host rocks.

The infiltrating silicate melts interact with carbonates, resulting in the 'exotic' compositions of glasses found in some skarn xenoliths. This may occur only at high temperature as indicated by melt inclusion data (800 °C < *T* < 1030 °C). High temperatures of formation for this type of skarn are also supported by the occurrence of melilite in some samples (stable above 950 °C at 100 MPa: Tracy & Frost, 1991) formed by the reaction:

$$\underset{\text{diopside}}{CaMgSi_2O_6} + \underset{\text{calcite}}{CaCO_3} \Leftrightarrow \underset{\text{akermanite (melilite group)}}{Ca_2MgSi_2O_7} + CO_2$$

These modified melts metasomatize the carbonates, inducing skarn reactions through reciprocal diffusion processes (Kerrick, 1977). This particular type of skarn found in Vesuvius xenoliths, which forms directly from the interaction between carbonate and high-temperature silicate melts, is called here magmatic skarn.

The sharp transition of salite-fassaite observed in some pyroxenes suggests their crystallization was initiated in uncontaminated melt and their growth continued following the reaction processes. Salitic cores can therefore be considered remnants of the solidification front. Temperatures of magmatic skarn formation, reported in Figure 4, are calculated by modelling the magma–carbonate interaction. Good agreement is observed between these values (Fig. 4) and experimental data obtained from the homogenization temperatures of melt inclusions in the 1944 magmatic skarn (Table 2).

Magmatic skarn formed in the 1944 reservoir in conjunction with fergusites and clinopyroxenites (respectively, the upper and lower portions of the magmatic reservoir), and in the lower and hotter portions (in conjunction with clinopyroxenites) of the AD 472 and AD 79 magma chambers.

5.b.2. Endoskarn

The occurrence of fluid inclusions in some skarn xenoliths, from AD 472 and AD 79 deposits, indicates circulation of a magmatic hypersaline fluid phase in the peripheral upper parts of the more evolved magma chambers. This is clearly confirmed by the evidence

https://doi.org/10.1017/S0016756804009392 Published online by Cambridge University Press

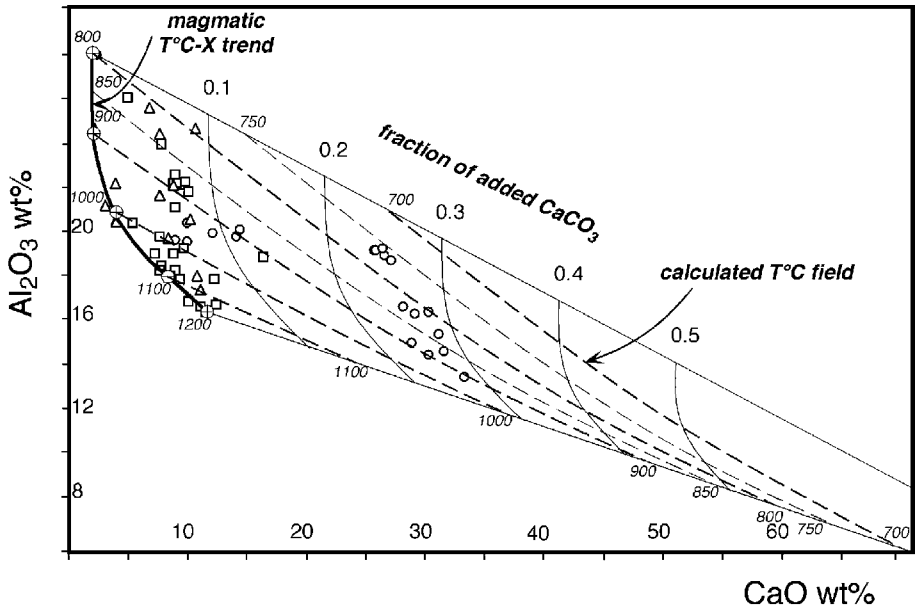

Figure 4. Al_2O_3 v. CaO plot of glasses and silicate melt inclusions from Vesuvius magmatic skarn. For legend see Figure 3. The magmatic trend was drawn after literature (Cioni *et al*. 1995; Cioni, Marianelli & Santacroce, 1998; Marianelli, Metrich & Sbrana, 1999) and new data on foid-bearing syenites and glass-bearing fergusites from the highly crystallized margins of magma chambers. The curves display the fraction of $CaCO_3$ added to magmatic melts through magma–host rock interactions. The suggested skarn thermal field is also indicated by dashed curves. The skarn thermal field was calculated by assuming thermal equilibrium between magma and carbonate country rocks. The processes taken into account in the calculation are cooling and crystallization of magma, and decarbonation of calcite according to the following reaction: $CaCO_3 = CaO(l) + CO_2(g)$. Initial temperature of carbonates is assumed to be 700 °C and its latent heat to be 1770 J/kg C, through the MELTS code (Ghiorso & Sack, 1995). The specific heats (including latent heat) of different magmatic compositions were also calculated through the MELTS code by using appropriate Vesuvius magma compositions.

of magmatic brine exsolution in foid-bearing syenites found in both eruptions.

The multiphase (carbonate-bearing) melt inclusions (Fig. 2b) found in the AD 472 skarn xenoliths are thought to result from a magmatic-derived hypersaline fluid that reacts with carbonate wall rocks (Fulignati *et al*. 2001), inducing carbonate melting through sintectic reactions (Lentz, 1998, 1999). This complex fluid (Na–K–Ca–carbonate–chloride-rich hydrosaline melt) metasomatizes the rigid crust (Fulignati *et al*. 2001) generating a typical endoskarn. The paucity of fluid inclusion-bearing xenoliths suggests that the exsolution of a hypersaline fluid phase is probably not extensive in the peripheral parts of the AD 472 chamber. As a consequence, the exsolved fluids are mainly confined at solidification front-carbonate wall rock interface of the 'young' magma chambers.

5.b.3. *Exoskarn*

In the more evolved AD 79 magma chamber, the exsolution of magmatic brines at the magma chamber margins is more developed, enhancing the infiltration of these fluids into the carbonate wall rocks. The presence of widespread skarn veins in xenolith marbles can be interpreted as strong evidence for infiltration metasomatism at the expense of carbonate protolith. The hypersaline fluid inclusions, found in AD 79 skarn xenoliths, are indicative of the infiltration metasomatism process that produces typical exoskarn. The infiltration of magmatic fluids into carbonate wall rocks is also favoured by the reactions between components (chloride compounds, silica, alumina, etc.) carried by magmatic fluids and carbonate. A typical reaction is:

$$FeCl_{2(aq)} + CaCO_3 + 2SiO_{2(aq)} + H_2O$$
$$\text{calcite}$$
$$\Leftrightarrow CaFeSi_2O_6 + CO_2 + 2HCl_{(aq)}$$
$$\text{hedenbergite}$$

(Kwak & Tan, 1981). These reactions produce calc-silicate minerals, CO_2 and HCl, the latter of which reacts with $CaCO_3$ according to the reaction:

$$2HCl_{(aq)} + CaCO_3 \Leftrightarrow CaCl_{2(aq)} + CO_2 + H_2O + \text{porosity}$$

(Kwak & Tan, 1981; Kwak, 1986), enhancing the permeability of the carbonate wall rocks.

https://doi.org/10.1017/S0016756804009392 Published online by Cambridge University Press

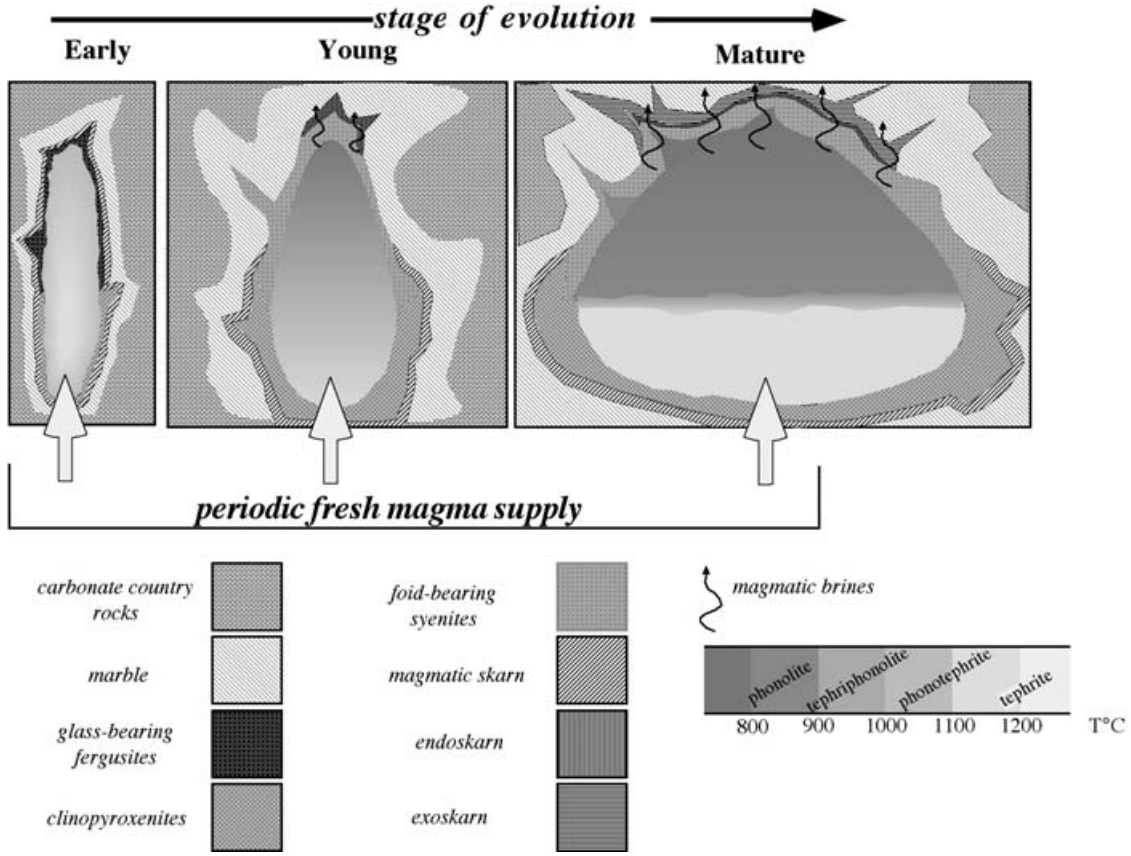

Figure 5. Sketch of the suggested magma chamber–metasomatic aureole relationships as a function of the evolutionary state of Vesuvian magmatic reservoirs. The figure is not to scale because the thickness of the skarn haloes has been magnified, indicating the different skarn type development in the different types of magma chambers.

5.b.4. Genesis of skarns associated with Vesuvius magma chambers

In summary (Fig. 5, Table 4), in the upper portion of the AD 472 and AD 79 magma chambers, endoskarn and exoskarn form and are related to the segregation and migration of hypersaline aqueous phase(s) from the crystallizing melts. Both types of skarn are produced by infiltrative transfer of components into the peripheral part of the chamber (endoskarn) and into carbonate host rock (exoskarn). Magmatic skarns (present in the 1944 and in the lower and hotter portions of AD 472 and AD 79 magma chambers) are instead dominated by melt–solid diffusion processes.

In general, the magmatic skarn v. endo-exoskarn volumetric ratio in the metasomatic aureoles depends on the prevailing skarn-forming mechanism (diffusive v. infiltrative fluid metasomatism) (Lentz, 1998). The transition between the most external part of the solidification front (rigid crust) and the skarn aureole is often observed at a centimetric to decimetric scale in Vesuvius xenoliths. Magmatic skarns are thought to be very thin, qualitatively in agreement with the thickness of exposed contact aureoles reported as being from <10 cm to 1–2 m (Joesten, 1977; Kerrick, 1977; Zhao & Zhao, 1996; Lentz, 1998). Where infiltrative fluid metasomatism prevails (exoskarn), the skarn halo might be more extensive, even if it is likely that exoskarn development will be mainly localized in veins because fluid discharging from the magma chamber will tend to be focused into permeable zones (fractures) in the wall rock.

In Vesuvius, the temperatures of skarn formation are always > 800 °C (Tables 2, 4), higher in magmatic skarn than in endo- and exoskarn. These high temperatures confirm that all investigated xenoliths are representative of prograde phases of skarn formation. The development of metasomatic aureoles is always induced by silicate melts or magmatic fluids formed on the walls of active magma chambers. All of this supports the idea that studied xenoliths come from margins of growing magma chambers and are not to be related to older magmatic reservoirs.

6. Conclusions

The frozen snapshots (xenoliths) of the magma chamber-mirroring skarn halo erupted from Vesuvius provide a rare opportunity to describe the state of a chamber and its sidewalls at a particular moment

https://doi.org/10.1017/S0016756804009392 Published online by Cambridge University Press

Table 4. Summary of data on the magma chamber-metasomatic aureole transition of Vesuvian magma chambers

Magma chambers		Solidification front	Metasomatic aureole	
Eruption	Magmas	Rock type	Skarn paragenesis	Skarn type
AD 79 'Mature' two-folded magma chamber ($\sim 4\ km^3$)[1]	Tephriphonolite ($T = 1000–1100\ ^\circ C$) and phonolite ($T = 850–900\ ^\circ C$)[3]	*Upper part* Foid-bearing syenites $T = \sim 830\ ^\circ C$	Fassaitic clinopyroxene + phlogopite + olivine + spinel + calcite + REE and HFSE-bearing accessories ± garnet ± plagioclase ± nepheline	Exoskarn $T = \sim 830\ ^\circ C$
		Lower part Cumulates (from clinopyroxenites to olivine-clinopyroxenites) $T < 1150\ ^\circ C$†	Fassaitic clinopyroxene + phlogopite + spinel ± olivine ± melilite	Magmatic skarn
AD 472 'Young' stratified magma chamber (0.5–1 km^3)[1]	Phonotephrite to phonolite ($T = 1120\ ^\circ C$ to $900\ ^\circ C$)[1]	*Upper part* Foid-bearing syenites $T = < 850\ ^\circ C$‡	Fassaitic clinopyroxene + phlogopite + nepheline + calcite	Endoskarn $T = \sim 800\ ^\circ C$
		Lower part Cumulates (from clinopyroxenites to olivine-clinopyroxenites) $T < 1150\ ^\circ C$†	Fassaitic clinopyroxene + melilite + phlogopite ± wollastonite Fassaitic clinopyroxene + phlogopite + spinel ± olivine	Magmatic skarn
1944 'Open conduit' homogeneous mafic magma crystal enriched downward magma chamber ($< 0.2\ km^3$)[2]	Mixing between tephrite and phonotephrite[2] ($T = 1200\ ^\circ C$ to $1060\ ^\circ C$)*	*Upper part* Glass-bearing fergusites $T \sim 1050\ ^\circ C$[4]	Fassaitic clinopyroxene + melilite + olivine + spinel ± plagioclase Fassaitic clinopyroxene + phlogopite + spinel + olivine ± plagioclase ± periclase	Magmatic skarn $T = \sim 1000\ ^\circ C$ Magmatic skarn $T = \sim 850\ ^\circ C$
		Lower part Cumulates (from clinopyroxenites to olivine-clinopyroxenites) $T < 1150\ ^\circ C$†	Fassaitic clinopyroxene + phlogopite + spinel ± olivine	Magmatic skarn

1 – Cioni, Marianelli & Santacroce (1998); 2 – Marianelli, Metrich & Sbrana (1999); 3 – Cioni *et al*. (1995); 4 – Fulignati *et al*. (2000):
* Temperatures are calculated by using the clinopyroxene geothermometer (Cioni, Marianelli & Santacroce, 1999).
† The upper limit of temperature of formation of cumulates are inferred from the homogenization temperatures of melt inclusions hosted in diopsides.
‡ Temperature estimated on the basis of homogenization temperatures of fluid inclusions, data from Fulignati *et al*. (2001) and this paper.

in time, and to significantly advance knowledge of metasomatic aureoles linked to different actively growing magma chambers.

Processes involved in the skarn genesis at the walls of Vesuvian magma chambers are controlled by the characteristics of magma reservoirs. The volatile-phase saturation and exsolution of hypersaline fluid phases from the crystallizing phonolitic upper parts of the 'young' (AD 472), and 'mature' (AD 79) Vesuvius magma chambers is one of the key processes that strongly constrains the development of the thermometamorphic–metasomatic aureole around the magma chambers. This is because the exsolved fluid phases are responsible for the transfer of reactants from the chamber into the wall rock. The infiltration of these fluids, and their interaction with carbonate, represents an effective mechanism for the development of 'endoskarn' (magmatic protolith) and 'exoskarn' (carbonate protolith). Less differentiated, hotter, modified melts, not having exsolved hypersaline fluid phases, promote the generation of 'magmatic skarn', through melt–solid diffusion processes in the 1944 reservoir, and in the lower and hotter parts of the more evolved magma chambers of Vesuvius.

In conclusion, the thermal-compositional conditions of the Vesuvius magma chambers clearly constrain the nature of the skarn aureoles (Fig. 5).

Acknowledgements. We are grateful to V. S. Kamenetsky for the critical reading of an early version of the manuscript. This paper benefited immensely from reviews by J. B. Lowenstern and J. Webster. Their constructive comments and suggestions greatly improved the quality and the clarity of the manuscript. We thank A. Longo for having calculated the skarn thermal field of Figure 4. This research was supported by a Gruppo Nazionale per la Vulcanologia-Istituto Nazionale di Geofisica e Vulcanologia grant.

References

BARBERI, F. & LEONI, L. 1980. Metamorphic carbonate ejecta from Vesuvius Plinian eruptions: evidence of the occurrence of shallow magma chambers. *Bulletin of Volcanology* **43**, 107–20.

BARBERI, F., BIZOUARD, H., CLOCCHIATTI, R., METRICH, N., SANTACROCE, R. & SBRANA, A. 1981. The Somma-Vesuvius magma chamber: a petrological and volcanological approach. *Bulletin of Volcanology* **44**, 295–315.

BELKIN, H. E. & DE VIVO, B. 1993. Fluid inclusion studies of ejected nodules from plinian eruptions of

https://doi.org/10.1017/S0016756804009392 Published online by Cambridge University Press

Mt. Somma-Vesuvius. *Journal of Volcanology and Geothermal Research* **58**, 89–100.

BELKIN, H. E., DE VIVO, B., ROEDDER, E. & CORTINI, M. 1985. Fluid inclusion geobarometry from ejected Mt. Somma-Vesuvius nodules. *American Mineralogist* **70**, 288–303.

BOWEN, N. L. 1928. *The evolution of igneous rocks*. Princeton, NJ: Princeton Univ. Press.

BURT, D. M. 1982. Skarn deposits – Historical bibliography through 1970. *Economic Geology* **77**, 755–63.

CIONI, R. 2000. Volatile content and degassing processes in the AD 79 magma chamber at Vesuvius (Italy). *Contributions to Mineralogy and Petrology* **140**, 40–54.

CIONI, R., CIVETTA, L., MARIANELLI, P., METRICH, N., SANTACROCE, R. & SBRANA, A. 1995. Compositional layering and syn-eruptive mixing of a periodically refilled shallow magma chamber: the AD 79 Plinian eruption of Vesuvius. *Journal of Petrology* **36**, 739–76.

CIONI, R., MARIANELLI, P. & SANTACROCE, R. 1998. Thermal and compositional evolution of the shallow magma chambers of Vesuvius: Evidence from pyroxene phenocrysts and melt inclusions. *Journal of Geophysical Research* **103**, 18277–94.

CIONI, R., MARIANELLI, P. & SANTACROCE, R.1999. Temperature of Vesuvius magmas. *Geology* **27**, 443–6.

CORTINI, M., LIMA, A. M. & DE VIVO, B. 1985.Trapping temperatures of melt inclusions from ejected Vesuvius mafic xenoliths. *Journal of Volcanology and Geothermal Research* **26**, 167–72.

EINAUDI, M. T., MEINERT, L. D. & NEWBERRY, R. J. 1981. Skarn deposits. *Economic Geology* **75**, 317–91.

FULIGNATI, P., KAMENETSKY, V. S., MARIANELLI, P., SBRANA, A. & MERNAGH, T. P. 2001. Melt inclusion record of immiscibility between silicate, hydrosaline, and carbonate melts: Applications to skarn genesis at Mount Vesuvius. *Geology* **29**, 1043–6.

FULIGNATI, P., KAMENETSKY, V. S., MARIANELLI, P. & SBRANA, A. 2004. Fluid inclusion evidence of second immiscibility within magmatic fluids (79 AD eruption of Mt. Vesuvius). *Periodico di Mineralogia*, in press.

FULIGNATI, P., MARIANELLI, P., SANTACROCE, R. & SBRANA, A. 2000. The skarn shell of the 1944 Vesuvius magma chamber. Genesis and P-T-X conditions from melt and fluid inclusion data. *European Journal of Mineralogy* **12**, 1025–39.

FULIGNATI, P., MARIANELLI, P. & SBRANA, A. 2000. Glass-bearing felsic nodules from the crystallizing sidewalls of the 1944 Vesuvius magma chamber. *Mineralogical Magazine* **64**, 481–96.

GHIORSO, M. S. & SACK, R. O. 1995. Chemical mass transfer in magmatic processes. IV. a revised and internally consistent thermodynamic model for the interpolation and extrapolation of liquid-solid equilibria in magmatic systems at elevated temperatures and pressures. *Contributions to Mineralogy and Petrology* **119**, 197–212.

GILG, H. A., LIMA, A., SOMMA, R., BELKIN, H. E., DE VIVO, B. & AYUSO, R. A. 2001. Isotope geochemistry and fluid inclusion study of skarns from Vesuvius. *Mineralogy and Petrology* **73**, 145–76.

JOESTEN, R. 1977. Mineralogical and chemical evolution of contaminated igneous rocks at gabbro-limestone contact, Christmas Mountains, Big Bend region, Texas. *Geological Society of America Bullettin* **88**, 1515–29.

KAMENETSKY, V. S., DE VIVO, B., NAUMOV, V. B., KAMENETSKY, M. B., MERNAGH, T. P., VAN ACHTERBERGH, E., RYAN, C. G. & DAVIDSON, P. 2003. Magmatic inclusions in the search for natural silicate-salt melt immiscibility: methodology and examples. In *Melt inclusions in volcanic systems: methods, applications and problems* (eds B. De Vivo and R. J. Bodnar), pp. 65–82. Development in Volcanology no. 5. Elsevier.

KERRICK, D. M. 1977. The genesis of zoned skarns in the Sierra Nevada, California. *Journal of Petrology* **18**, 144–81.

KWAK, T. A. P. 1986. Fluid inclusions in skarns (carbonate replacement deposits). *Journal of Metamorphic Geology* **4**, 363–84.

KWAK, T. A. P. & TAN, T. H. 1981. The importance of $CaCl_2$ in fluid composition trends-evidence from the King Island (Dolphin) skarn deposit. *Economic Geology* **76**, 955–60.

LE BAS, M. J., LE MAITRE, R. W., STRECKEISEN, A. & ZANETTIN, A. 1986. A chemical classification of volcanic rocks based on the total alkali-silica diagram. *Journal of Petrology* **27**, 745–50.

LENTZ, D. R. 1998. Late-tectonic U-Th-Mo-REE skarn and carbonatitic vein-dyke systems in the southwestern Grenville Province: a pegmatite-related pneumatolytic model linked to marble melting (limestone syntexis). In *Mineralized intrusion-related skarn systems* (ed. D. R. Lentz), pp. 519–657. *Mineralogical Association of Canada Short Course* **26**.

LENTZ, D. R. 1999. Carbonatite genesis: A reexamination of the role of intrusion-related pneumatolytic skarn processes in limestone melting. *Geology* **27**, 335–8.

LIMA, A. M., DANYUSHEVSKY, L. V., DE VIVO, B. & FEDELE, L. 2003. A model for the evolution of the Mt. Somma-Vesuvius magmatic system based on fluid and melt inclusion investigations. In *Melt inclusions in volcanic systems: methods, applications and problems* (eds B. De Vivo and R. J. Bodnar), pp. 227–49. Development in Volcanology no. 5. Elsevier.

LOWENSTERN, J. B. 1995. Application of silicate-melt inclusions to the study of magmatic volatiles. In *Magmas, fluids, and ore deposits* (ed. J. F. H. Thompson), pp. 71–99. *Mineralogical Association of Canada Short Course* **23**.

LOWENSTERN, J. B. & SINCLAIR, W. D. 1996. Exsolved magmatic fluid and its role in the formation of comb-layered quartz at the Cretaceous Logtung W-Mo deposit, Yukon Territory, Canada. *Transactions of the Royal Society of Edinburgh: Earth Sciences* **87**, 291–303.

MARIANELLI, P. & SBRANA, A. 1998. Risultati di misure standard di minerali e di vetri naturali in microanalisi a dispersione di energia. *Atti della Societoà Toscana di Scienze Naturali* **105**, 57–63.

MARIANELLI, P., METRICH, N., SANTACROCE, R. & SBRANA, A. 1995. Mafic magma batches at Vesuvius: a glass inclusion approach to the modalities of feeding strato-volcanoes. *Contributions to Mineralogy and Petrology* **120**, 159–69.

MARIANELLI, P., METRICH, N. & SBRANA, A. 1999. Shallow and deep reservoirs involved in magma supply of the 1944 eruption of Vesuvius. *Bulletin of Volcanology* **61**, 48–63.

MARSH, B. D. 1995. Solidification fronts and magmatic evolution. *Mineralogical Magazine* **60**, 5–40.

MATTHEWS, S. J., MARQUILLAS, R. A., KEMP, A. J., GRANGE, F. K. & GARDEWEG, M. C. 1996. Active skarn formation

beneath Lascar Volcano, northern Chile: a petrographic and geochemical study of xenoliths in eruption products. *Journal of Metamorphic Geology* **14**, 509–30.

MEINERT, L. D. 1992. Skarns and skarn deposits. *Geoscience Canada* **19**, 145–62.

MEINERT, L. D. 1993. Igneous petrogenesis and skarn deposits. In *Mineral Deposit Modeling* (eds R. V. Kirkam, W. D. Sinclair, R. I. Thorpe and J. M. Duke), pp. 569–83. Geological Association of Canada, Special Paper no. 40.

ROEDDER, E. 1992. Fluid inclusion evidence for immiscibility in magmatic differentiation. *Geochimica et Cosmochimica Acta* **56**, 5–20.

SANTACROCE, R., BERTAGNINI, A., CIVETTA, L., LANDI, P. & SBRANA, A. 1993. Eruptive dynamics and petrogenetic processes in a very shallow magma reservoir. *Journal of Petrology* **34**, 383–425.

SOBOLEV, A. V., DMITREV, L. V., BARSUKOV, V. L., NEVSOROV, V. N. & SLUTSKY, A. V. 1980. The formation conditions of high magnesium olivines from the monomineral fraction of Luna-24 regolith., Lunar and Planetary Science Conference 11th, New York, pp. 105–16. Pergamon Press.

STERNER, S. M., HALL, D. L. & BODNAR, R. J. 1988. Synthetic fluid inclusions. V. Solubility relations in the system NaCl-KCl-H_2O under vapour-saturated conditions. *Geochimica et Cosmochimica Acta* **52**, 989–1006.

TRACY, R. J. & FROST, B. R. 1991. Phase equilibria and thermobarometry of calcareous, ultramafic and mafic rocks, and iron formations. In *Contact metamorphism* (ed. D. M. Kerrick), pp. 207–89. *Reviews in Mineralogy* **26**.

WEBSTER, J. D. & DE VIVO, B. 2002. Experimental and modeled solubilities of chlorine in aluminosilicate melts, consequences of magma evolution, and implications for exsolution of hydrous chloride melt at Mt. Somma-Vesuvius. *American Mineralogist* **87**, 1046–61.

WEBSTER, J. D., DE VIVO, B. & TAPPEN, C. 2003. Volatiles, magmatic degassing and eruptions of Mt. Somma-Vesuvius: constraints from silicate melt inclusions, Cl and H_2O solubility experiments and modeling. In *Melt inclusions in volcanic systems: methods, applications and problems* (eds B. De Vivo and R. J. Bodnar), pp. 207–26. Development in Volcanology no. 5. Elsevier.

WEBSTER, J. D., RAIA, F., DE VIVO, B. & ROLANDI, G. 2001. The behavior of chlorine and sulfur during differentiation of the Mt. Somma-Vesuvius magmatic system. *Mineralogy and Petrology* **73**, 177–200.

WOHLETZ, K. H. 2002. *KWare Magma* (version 2.46.0088). University of California, Los Alamos Laboratories.

ZHAO BIN & ZHAO JINSONG. 1996. Main geological and geochemical characteristics of massive calcareous skarns from middle-lower reaches of Yangtze River. *Progress in Geochemistry, Symposium Proceedings International Geological Congress 1996, Beijing China*, 26–52.

ZHAO JINSONG & NEWBERRY, R. J. 1996. Novel knowledge on the origin and mineralization of skarns from Shizhuyuan. *Acta Mineralogica Sinica* **16**, 441–9 (in Chinese with English abstract.)

ZHAO JINSONG, ZHAO BIN & LI ZHAO-LIN 2000. Finding of melt inclusion in skarn mineral from Daye iron deposit and its geologic-geochemical significance. *Geochimica* **29**, 500–3 (in Chinese with English abstract.)